# 12 - volume growth
# cardiac growth




## heart disease

- primary cause of death in industrialized nations
- affects 80 mio americans
- damaged cardiac tissue does not self regenerate

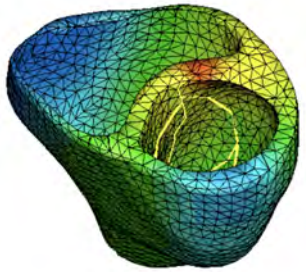

## forms of cardiac growth

- case I - athlete's heart
  stress driven isotropic growth
- case II - cardiac dilation
  strain driven eccentric growth
- case III - cardiac wall thickening
  stress driven concentric growth



## organ level - human heart and its characteristic microstructure

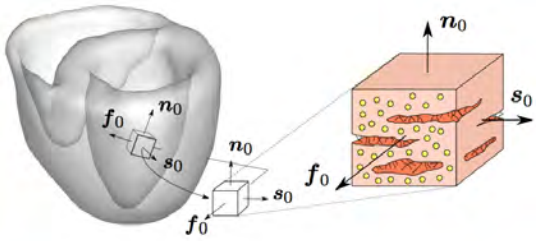


**Figure 1**. Normal healthy heart, courtesy of Chengpei Xu (left). Microstructural architecture of the heart (right). The orthogonal unit vectors $f_0$ and $s_0$ designate the muscle fiber direction and the sheet plane vector in the undeformed configuration. The orthogonal vector $n_0$ completes the local coordinate system, where the constitutive response of the heart is typically viewed as orthotropic.

goktepe, abilez, kuhl [2010]



## cellular level - cardiomyocyte and its characteristic microstructure

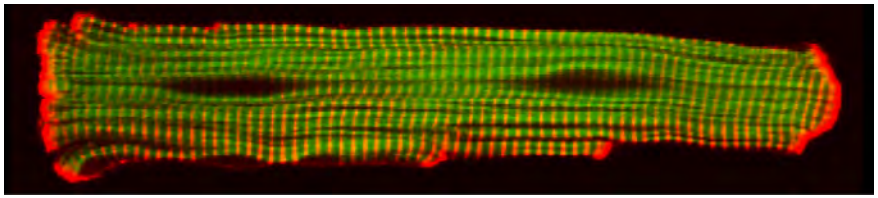

**Figure 1**. Adult ventricular cardiomyocyte. The sarcomeric actin is labeled in green and the periodically spaced t-tubule system is marked in red, giving the cell its characteristic striated appearance. Healthy cardiomyocytes have a cylindrical shape with a diameter of 10-25µm and a length of 100µm, consisting of approximately 50 sarcomere units in series making up a myofibril and 50-100 myofibrils in parallel. Cardiac disease can be attributed to structural changes in the cardiomyocyte, either through eccentric growth in dilated cardiomyopathy or through concentric growth in hypertrophic cardiomyopathy.

kevin kit parker, disease biophysics group, harvard

## molecular level - sarcomere and its characteristic microstructure

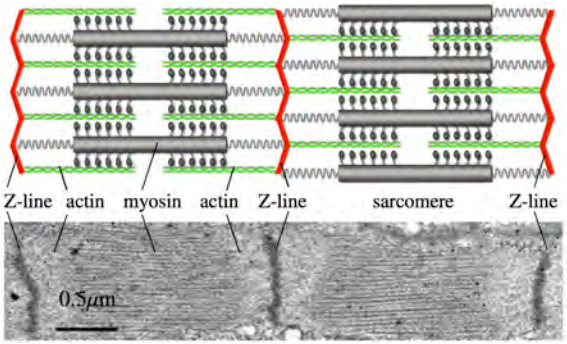


**Figure 2**. Sarcomere units of human embryonic stem cell-derived cardiomyocyte. Sarcomeres are defined as the segment between two neighboring Z-lines, shown in red, which appear as dark lines under the transmission electron microscope. Healthy sarcomeres are 1.9-2.1μm long characterized through a parallel arrangement of thick filaments of myosin, displayed in grey, sliding along thin filaments of actin, labeled in green. Although cardiac cells are known to change length and thickness in response to mechanical loading, the individual sarcomeres maintain an optimal resting length.

goktepe, abilez, parker, kuhl [2010]



## organ level - pathophysiology of maladaptive growth

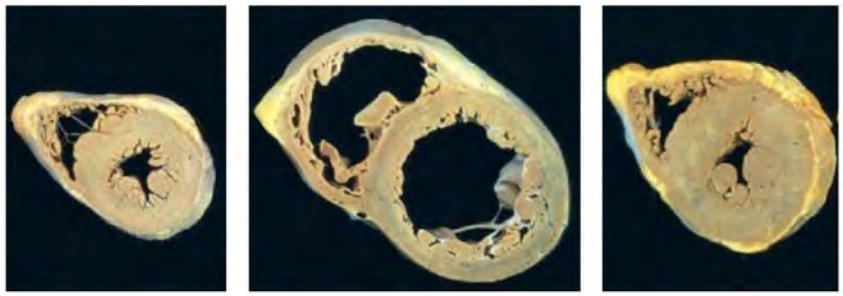

**Figure 2**. Pathophysiology of maladaptive growth of the heart viewed in transverse heart sections, reprinted with permission from Robbins & Cotran. Compared with the normal heart (left), eccentric hypertrophy is associated with ventricular dilation in response to volume overload (center). Concentric hypertrophy is associated with ventricular wall thickening in response to pressure overload (right).

kumar, abbas, fausto [2005]



## cellular level - pathophysiology of maladaptive growth

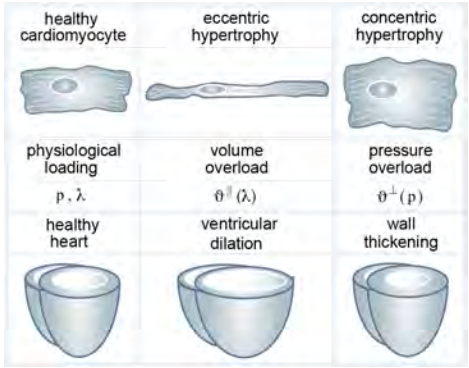


**Figure 3**. Eccentric and concentric growth on the cellular and organ levels. Compared with the normal heart (left), volume-overload induced eccentric hypertrophy is associated with cell lengthening through the serial deposition of sarcomere units and manifests itself in ventricular dilation in response to volume-overload (center). Pressure-overload induced concentric hypertrophy is associated with cell thickening through the parallel deposition of sarcomere units and manifests itself in ventricular wall thickening in response to pressure-overload (right).

goktepe, abilez, parker, kuhl [2010]



## molecular level - pathophysiology of maladaptive growth

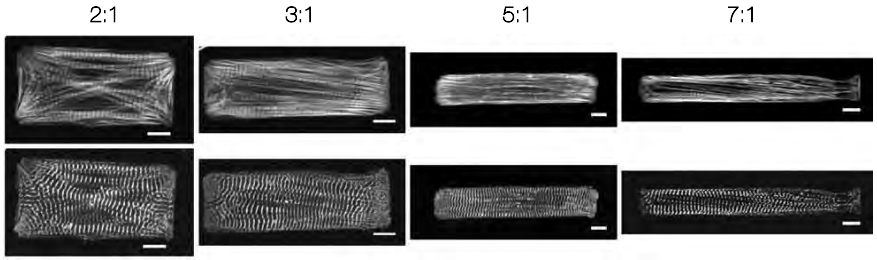


**Figure 3**.Controlled cardiomyocyte remodeling in vitro. Cardiomyocytes adapt their size, shape, and intracellular architecture when spatially confined in vitro through patterning on fibronactin islands at different aspect ratios (2:1, 3:1, 5:1, and 7:1). Isolated confocal slices display 2D morphology of myofibrils with respect to actin (top) and alpha-actinin (bottom). Although overall cardiomyocyte size changes, the individual sarcomere units remain at constant length.

geisse, sheehy, parker [2009]

## linking growth across the scales - fiber orientation

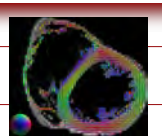

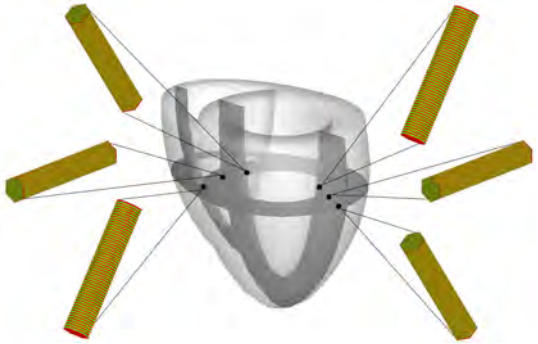

**Figure 6**. Generic biventricular heart model generated from two truncated ellipsoids, with heights of 70mm and 60mm, radii of 30mm and 51mm, and wall thicknesses of 12mm and 6mm, respectively. In the healthy heart, cardiomycytes are assumed to be cylindrical, 100µm long with a diameter of 16.7µm. They consist of 50 serial sarcomere units in length and 91 parallel units per cross section, each of them 2µm long and 2µm in diameter. They are arranged helically around the long axis of the heart with a transmurally varying inclination of -55° in the epicardium, the outer wall, to +55° in the endocardium, the inner wall, measured with respect to the basal plane.

göktepe, abilez, parker, kuhl [2010], collaboration with dan ennis, dept radiology, UCLA

## motivation - cardiac growth



## kinematics of finite growth

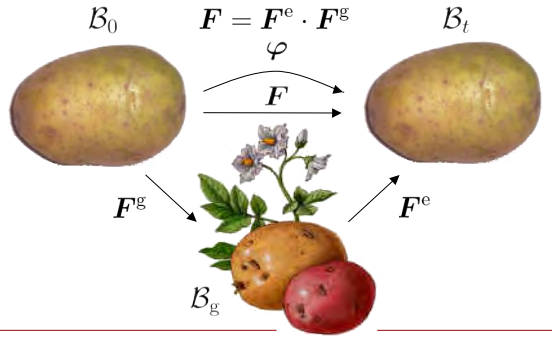


## concept of incompatible growth configuration

lee [1969], rodriguez, hoger, mc culloch [1994], taber [1995], epstein, maugin [2000], humphrey [2002], ambrosi, mollica [2002], himpel, kuhl, menzel, steinmann [2005]

## motivation - cardiac growth



## locally orthotropic material behavior

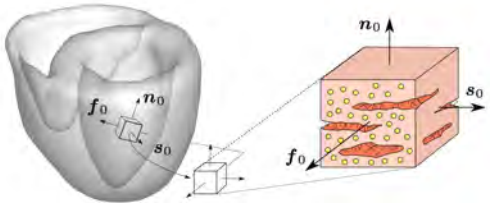


$$\psi = \kappa\,[J^{\mathrm{e}} - \ln(J^{\mathrm{e}}) - 1] + \frac{a}{2b}\,\exp(b[I_1^{\mathrm{e}} - 3])$$
$$+ \frac{a_{\mathrm{s}}}{2b_{\mathrm{s}}}[\exp(b_{\mathrm{s}}[I_{\mathrm{s}}^{\mathrm{e}} - 1]^2) - 1] + \frac{a_{\mathrm{f}}}{2b_{\mathrm{f}}}[\exp(b_{\mathrm{f}}[I_{\mathrm{f}}^{\mathrm{e}} - 1]^2) - 1] + \frac{a_{\mathrm{fs}}}{2b_{\mathrm{fs}}}[\exp(b_{\mathrm{fs}}\, I_{\mathrm{fs}}^{\mathrm{e}\,2}) - 1]$$

$$\boldsymbol{\tau} = 2\frac{\partial \psi}{\partial \boldsymbol{g}} = J^{\mathrm{e}}\, p\, \boldsymbol{g}^{-1} + 2\,\psi_1'\ \boldsymbol{b}^{\mathrm{e}} + 2\,\psi_{\mathrm{f}}'\ \boldsymbol{f}^{\mathrm{e}} \otimes \boldsymbol{f}^{\mathrm{e}}$$
$$+ 2\,\psi_{\mathrm{fs}}'[\boldsymbol{f}^{\mathrm{e}} \otimes \boldsymbol{s}^{\mathrm{e}}]^{\mathrm{sym}} + 2\,\psi_{\mathrm{s}}'\,\boldsymbol{s}^{\mathrm{e}} \otimes \boldsymbol{s}^{\mathrm{e}}$$

dokos, smaill, young, le griece [2002], schmid, nash, young, hunter [2006], holzapfel, ogden [2009], göktepe, acharya, wong, kuhl [2010]

## constitutive equations



## locally orthotropic material behavior

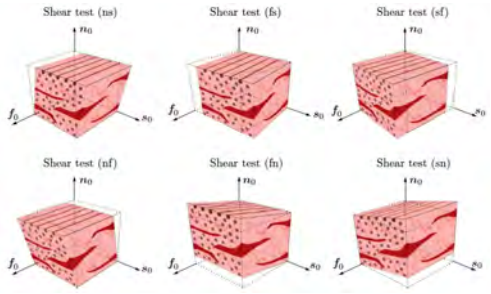


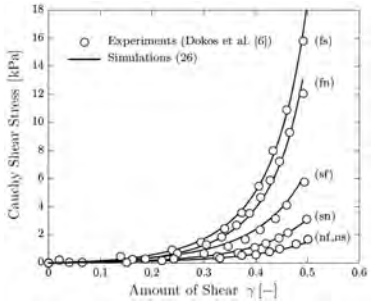


dokos, smaill, young, le griece [2002], schmid, nash, young, hunter [2006], holzapfel, ogden [2009], göktepe, acharya, wong, kuhl [2010]

## constitutive equations

## locally orthotropic material behavior

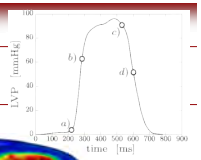


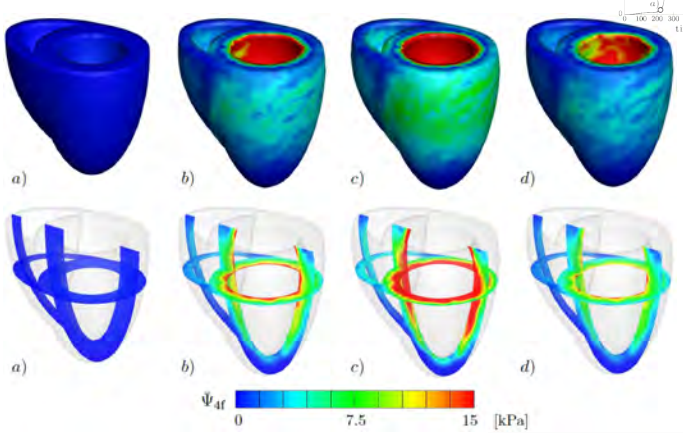


göktepe, acharya, wong, kuhl [2010]



## locally orthotropic material behavior

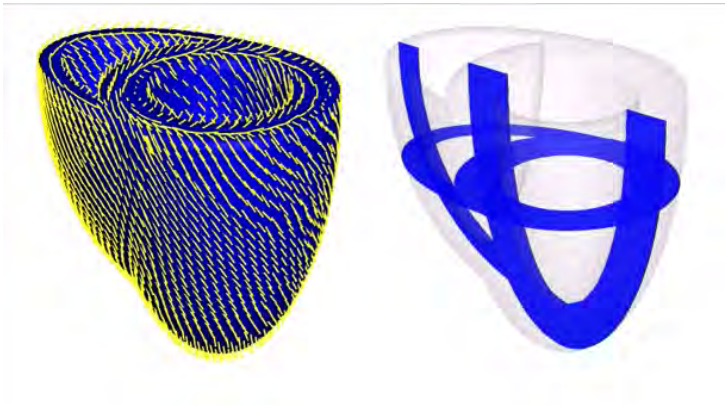

göktepe, acharya, wong, kuhl [2010]



## case I - athlete's heart syndrome

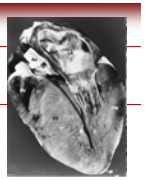

- growth due to **significant exercise**
- driven by **elevated pressure** and **increased filling**

- cardiac **output increases** from 6 l/min at rest **to 40 l/min**
- cardiac **mass increases** up to **50%**

- cardiomyocyte number remains constant ~6 billion
- cardiomyocyte **size increases isotropically up to 40%**

eckblom, hermansen [1968], hunter, chien [1999], plum, zwinderman, van der laarse, van der wall [2000]



## first reported case of heart failure in athletes

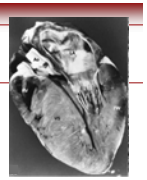



the word **marathon** originates from the **legend of phidippides**. phidippides was sent from the battlefield of marathon to athens to announce that the persians who had invaded greece had been defeated in the battle of marathon. the legend states that pheidippides ran the entire **distance of 26 miles** without stopping and burst into the assembly, to announce greece's victory before he **collapsed and died on the spot**. [490bc]

## physiology of athlete's heart

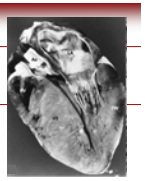

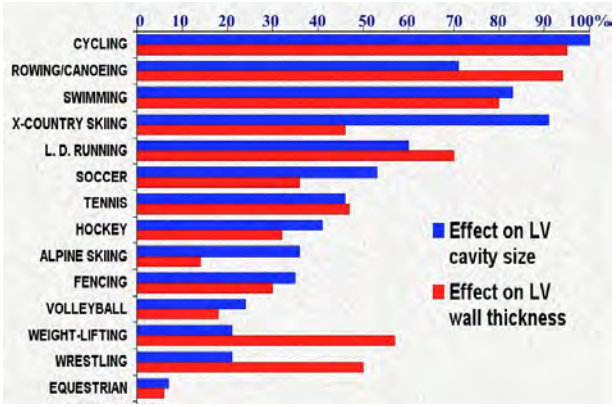


**Table**. Relative impact of different sports on left ventricular (LV) dimensions.

pelliccia [1998]



## governing equations

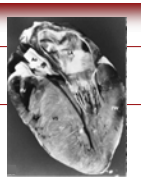

- multiplicative decomposition
  $\boldsymbol{F} = \boldsymbol{F}^{\mathrm{e}} \cdot \boldsymbol{F}^{\mathrm{g}}$ with $\boldsymbol{F} = \nabla_{\boldsymbol{X}} \boldsymbol{\varphi}$
- growth tensor
  $\boldsymbol{F}^{\mathrm{g}} = \vartheta^{\mathrm{g}} \boldsymbol{I}$
- evolution of isotropic growth multiplier
  cardiomyocyte volume increase rate
  $\dot{\vartheta}^{\mathrm{g}} = k^{\mathrm{g}}(\vartheta^{\mathrm{g}})\, \phi^{\mathrm{g}}(\boldsymbol{M}^{\mathrm{e}})$ with $k^{\mathrm{g}}(\vartheta^{\mathrm{g}}) = \frac{1}{\tau} \left[ \frac{\vartheta^{\max} - \vartheta^{\mathrm{g}}}{\vartheta^{\max} - 1} \right]^{\gamma}$
- growth criterion
  $\phi^{\mathrm{g}} = \mathrm{tr}(\boldsymbol{M}^{\mathrm{e}}) - M^{\mathrm{e\,crit}}$

maximum cardiomyocyte increase $\vartheta^{\max}$, sarcomere deposition time $\tau$, deposition nonlinearity $\gamma$, critical pressure level $M^{\mathrm{e\,crit}}$



## four parameter growth model - sensitivity analysis

$\phi^{\mathrm{g}} = \mathrm{tr}(\boldsymbol{M}^{\mathrm{e}}) - M^{\mathrm{e\,crit}}$ $\quad k^{\mathrm{g}}(\vartheta^{\mathrm{g}}) = [[\vartheta^{\max} - \vartheta^{\mathrm{g}}] / [\vartheta^{\max} - 1]]^{\gamma} / \tau$

maximum cardiomyocyte increase $\vartheta^{\max}$ sarcomere deposition time $\tau$

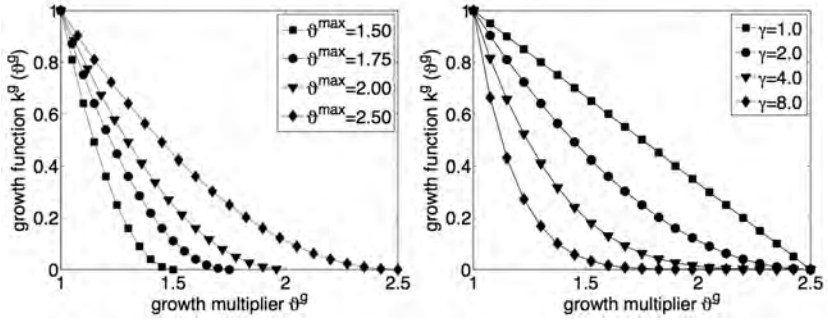


**Figure 5**. Three-parameter growth function. The growth rate decays smoothly until the growth multiplier $\vartheta$ has reached its maximum value $\vartheta^{max}$, here shown for $\gamma = 2.0$ and $\tau = 1.0$ (left). The nonlinearity of the growth process increases for increasing $\gamma$, here shown for $\gamma = 2.5$ and $\tau = 1.0$.

goktepe, abilez, kuhl [2010]



## algorithmic treatment

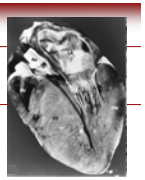

| | |
|---|---|
| given $\boldsymbol{F}$ and $\vartheta^{\mathrm{g}}_{\mathrm{n}}$ | |
| initialize $\vartheta^{\mathrm{g}} \leftarrow \vartheta^{\mathrm{g}}_{\mathrm{n}}$ | |
| local Newton iteration | |
| calculate elastic tensor $\boldsymbol{F}^{\mathrm{e}} = \boldsymbol{F} / \vartheta^{\mathrm{g}}$ | (1) |
| calculate elastic right Cauchy Green tensor $\boldsymbol{C}^{\mathrm{e}} = \boldsymbol{F}^{\mathrm{e\,t}} \cdot \boldsymbol{F}^{\mathrm{e}}$ | (2) |
| calculate second Piola Kirchhoff stress $\boldsymbol{S}^{\mathrm{e}} = 2\,\partial\psi / \partial \boldsymbol{C}^{\mathrm{e}}$ | (10) |
| check growth criterion $\phi^{\mathrm{g}} = \mathrm{tr}(\boldsymbol{C}^{\mathrm{e}} \cdot \boldsymbol{S}^{\mathrm{e}}) - M^{\mathrm{e\,crit}} \geq 0$ ? | (29) |
| calculate growth function $k^{\mathrm{g}} = [[\vartheta^{\max} - \vartheta^{\mathrm{g}}]/[\vartheta^{\max} - 1]]^{\gamma} / \tau$ | (28) |
| calculate residual $\mathsf{R} = \vartheta^{\mathrm{g}} - \vartheta^{\mathrm{g}}_{\mathrm{n}} - k^{\mathrm{g}}\, \phi^{\mathrm{g}} \Delta t$ | (30) |
| calculate tangent $\mathsf{K} = \partial \mathsf{R} / \partial \vartheta^{\mathrm{g}}$ | (31) |
| update growth multiplier $\vartheta^{\mathrm{g}} \leftarrow \vartheta^{\mathrm{g}} - \mathsf{R} / \mathsf{K}$ | |
| check convergence $\mathsf{R} \leq$ tol ? | |
| calculate second Piola Kirchhoff stress $\boldsymbol{S} = 1 / \vartheta^{\mathrm{g}\,2}\, \boldsymbol{S}^{\mathrm{e}}$ | (32) |
| calculate Lagrangian moduli $\mathsf{L}$ | (35) |
| push forward to Kirchhoff stresses $\boldsymbol{\tau} = \boldsymbol{F} \cdot \boldsymbol{S} \cdot \boldsymbol{F}^{\mathrm{t}}$ | (36) |
| push forward to Eulerian moduli $\mathbf{e} = [\boldsymbol{F} \boxtimes \boldsymbol{F}] : \mathsf{L} : [\boldsymbol{F}^{\mathrm{t}} \boxtimes \boldsymbol{F}^{\mathrm{t}}]$ | (37) |

**Table 1**. Algorithmic treatment of stress-driven isotropic growth.

goktepe, abilez, kuhl [2010]

## physiology of athlete's heart syndrome

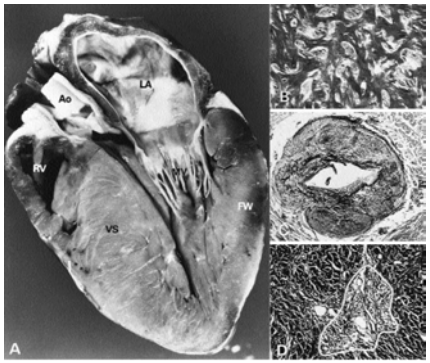


**Figure**. Morphological components of the disease process in hypertrophic cardiomyopathy (HCM), the most common cause of sudden death in young competitive athletes. A. Gross heart specimen sectioned in cross-sectional plane; left ventricular wall thickening shows an asymmetrical pattern and is confined primarily to the ventricular septum, which bulges prominently into the left ventricular outflow tract. the levt ventricular cavity appears in reduced size. B-D Histological features characteristic of left ventricular myocardium in HCM.

maron [1997]

## athlete's heart - isotropic growth



## athlete's heart - stress-driven isotropic growth

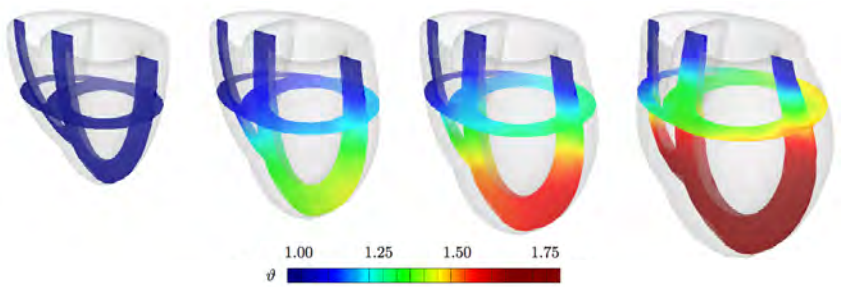


**Figure 7**. Athlete's heart, stress-driven isotropic eccentric and concentric growth, left ventricular dilation and wall thickening. The isotropic growth multiplier gradually increases from 1.00 to 1.75 as the individual cardiomyocytes grow both eccentrically and concentrically. On the macroscopic scale, the athlete's heart manifests itself in a progressive apical growth with a considerably increase in left ventricular cavity size to enable increased cardiac output during excercise. To withstand higher blood pressure levels during training, the heart muscle grows and the wall thickens.

goktepe, abilez, kuhl [2010]

## athlete's heart - isotropic growth



## case II - cardiac dilation

- chronic **enlargement** at constant wall thickness
- cardiac **mass increases 3x** to 1000 g
- cardiomyocyte number remains constant ~6 billion
- cardiomyocytes **lengthen 40%** at constant cell diameter
- sarcomere number increases **from ~50 to ~70** in series
- sarcomere length remains constant at 1.9-2.1um

eckblom, hermansen [1968], gerdes et al [1992], hunter, chien [1999], plum et al [2000], yoshida et al [2010]

## cardiac dilation - eccentric growth



## case II - cardiac dilation

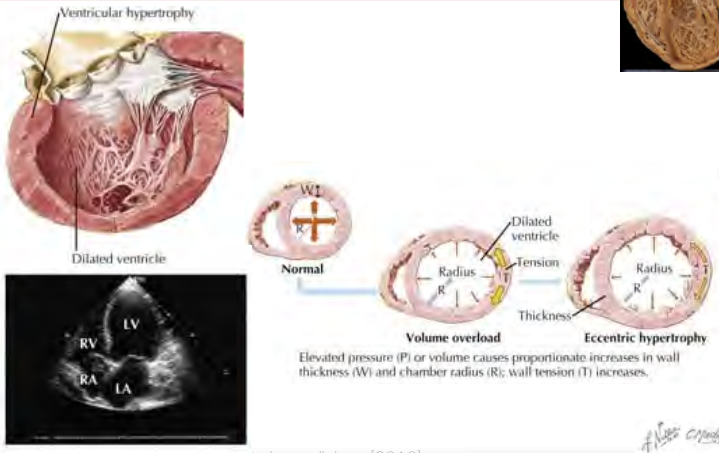


netter's cardiology [2010]

## cardiac dilation - eccentric growth

## constitutive equations

- multiplicative decomposition

$$\boldsymbol{F} = \boldsymbol{F}^{\mathrm{e}} \cdot \boldsymbol{F}^{\mathrm{g}} \qquad \text{with} \quad \boldsymbol{F} = \nabla_{\boldsymbol{X}} \boldsymbol{\varphi}$$

- growth tensor

$$\boldsymbol{F}^{\mathrm{g}} = \boldsymbol{I} + [\,\lambda^{\mathrm{g}} - 1\,]\, \boldsymbol{f}_0 \otimes \boldsymbol{f}_0$$

- evolution of eccentric growth multiplier
  serial sarcomere deposition rate

$$\dot{\lambda}^{\mathrm{g}} = k^{\mathrm{g}}(\lambda^{\mathrm{g}})\, \phi^{\mathrm{g}}(\lambda^{\mathrm{e}}) \qquad \text{with} \quad k^{\mathrm{g}} = \frac{1}{\tau} \left[ \frac{\lambda^{\max} - \lambda^{\mathrm{g}}}{\lambda^{\max} - 1} \right]^{\gamma}$$

- growth criterion

$$\phi^{\mathrm{g}} = \lambda^{\mathrm{e}} - \lambda^{\mathrm{crit}} = \frac{\lambda}{\lambda^{\mathrm{g}}} - \lambda^{\mathrm{crit}}$$

maximum serial sarcomere deposition $\lambda^{\max}$, sarcomere deposition time $\tau$, deposition nonlinearity $\gamma$, critical sarcomere stretch $\lambda^{\mathrm{crit}}$



## algorithmic treatment

| | |
|---|---|
| given $\boldsymbol{F}$ and $\lambda^{\mathrm{g}}_{\mathrm{n}}$ | |
| initialize $\lambda^{\mathrm{g}} \leftarrow \lambda^{\mathrm{g}}_{\mathrm{n}}$ | |
| local Newton iteration | |
| check growth criterion $\phi^{\mathrm{g}} = \lambda^{\mathrm{e}} - \lambda^{\mathrm{crit}} \geq 0$ ? | (46) |
| calculate growth function $k^{\mathrm{g}} = [[\lambda^{\max} - \lambda^{\mathrm{g}}]/[\lambda^{\max} - 1]]^{\gamma} / \tau$ | (45) |
| calculate residual $\mathsf{R} = \lambda^{\mathrm{g}} - \lambda^{\mathrm{g}}_{\mathrm{n}} - k^{\mathrm{g}}\, \phi^{\mathrm{g}} \Delta t$ | (47) |
| calculate tangent $\mathsf{K} = \partial \mathsf{R} \,/\, \partial \partial^{\mathrm{g}}$ | (48) |
| update growth stretch $\lambda^{\mathrm{g}} \leftarrow \lambda^{\mathrm{g}} - \mathsf{R} \,/\, \mathsf{K}$ | |
| check convergence $\mathsf{R} \leq$ tol ? | |
| calculate growth tensor $\boldsymbol{F}^{\mathrm{g}} = \boldsymbol{I} + [\lambda^{\mathrm{g}} - 1] \boldsymbol{f}_0 \otimes \boldsymbol{f}_0$ | (41) |
| calculate elastic tensor $\boldsymbol{F}^{\mathrm{e}} = \boldsymbol{F} \cdot \boldsymbol{F}^{\mathrm{g}\,-1}$ | (1) |
| calculate elastic right Cauchy Green tensor $\boldsymbol{C}^{\mathrm{e}} = \boldsymbol{F}^{\mathrm{e}\,\mathrm{t}} \cdot \boldsymbol{F}^{\mathrm{e}}$ | (2) |
| calculate elastic second Piola Kirchhoff stress $\boldsymbol{S}^{\mathrm{e}} = 2\, \partial \psi \,/\, \partial \boldsymbol{C}^{\mathrm{e}}$ | (10) |
| calculate second Piola Kirchhoff stress $\boldsymbol{S} = \boldsymbol{F}^{\mathrm{g}\,-1} \cdot \boldsymbol{S}^{\mathrm{e}} \cdot \boldsymbol{F}^{\mathrm{g}}$ | (17) |
| calculate Lagrangian moduli $\mathbb{L}$ | (18) with (19), (20), (43), (49) |
| push forward to Kirchhoff stress $\boldsymbol{\tau} = \boldsymbol{F} \cdot \boldsymbol{S} \cdot \boldsymbol{F}^{\mathrm{t}}$ | (21) |
| push forward to Eulerian moduli $\mathbb{e} = [\boldsymbol{F} \otimes \boldsymbol{F}] : \mathbb{L} : [\boldsymbol{F}^{\mathrm{t}} \otimes \boldsymbol{F}^{\mathrm{t}}]$ | (22) |

**Table 2**. Algorithmic treatment of strain-driven transversely isotropic growth.

goktepe, abilez, kuhl [2010]



## pathophysiology of cardiac dilation

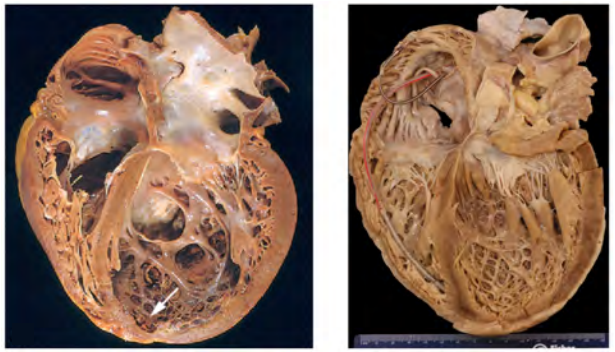

**Figure 8**. Strain-driven eccentric growth, cardiac dilation, and increase in cavity size at constant wall thickness. The heart is usually enlarged, rounded, flabby, and heavy with a weight of up to three times its normal weight (left), reprinted with permission from Robbins and Cotran. Heart specimen from a patient with cardiac dilation who died in end-stage heart failure. The ventricles are significantly dilated while the wall thickness has remained unaltered, courtesy of Allen P. Burke.

goktepe, abilez, kuhl [2010]



## cardiac dilation through strain-driven eccentric growth

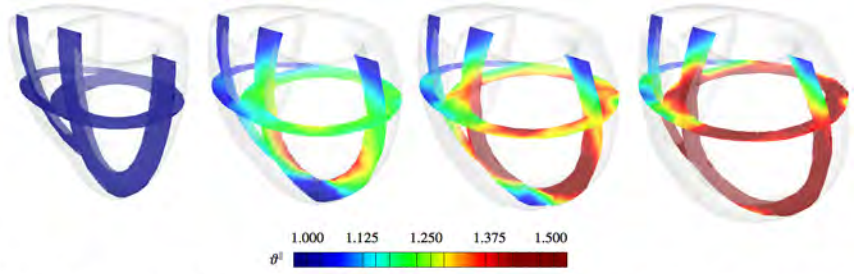


**Figure 10**. Strain-driven eccentric growth. The eccentric growth multiplier gradually increases from 1.00 to 1.50 as the individual cardiomyocytes grow eccentrically. On the structural level, eccentric growth manifests itself in a progressive dilation of the left ventricle accompanied by a significant increase in cardiac mass, while the thickness of the ventricular wall remains virtually unchanged.

goktepe, abilez, parker, kuhl [2010]

## cardiac dilation through strain-driven eccentric growth

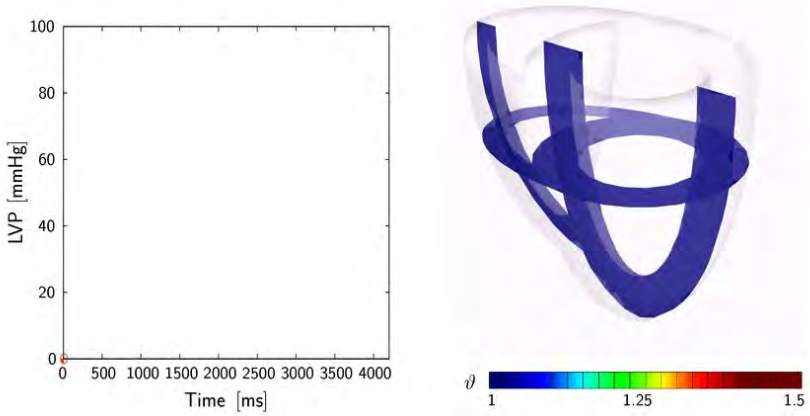


göktepe, abilez, parker, kuhl [2010]

## cardiac dilation - eccentric growth



## *in vivo* model of cardiac dilation

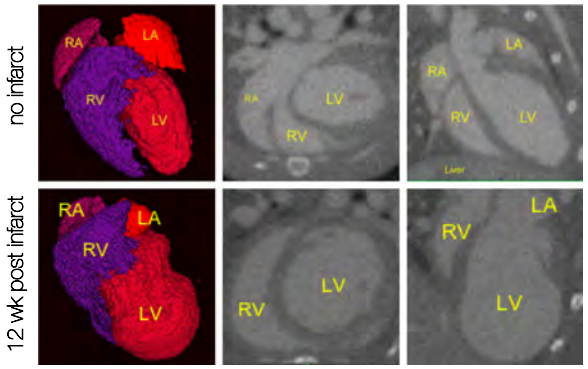


end-diastolic volume ↑ from 37.12mm$^3$ to 133.16mm$^3$

doyle, sheikh, sheikh, cao, yang, robbins, wu [2007]

## cardiac dilation - eccentric growth



## *in vivo* model of cardiac dilation

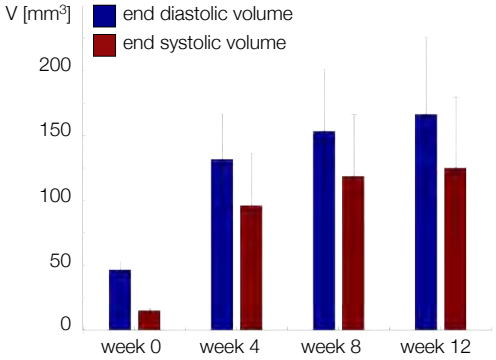


ejection fraction ↓ from 68.16% to 23.33%

doyle, sheikh, sheikh, cao, yang, robbins, wu [2007]

## cardiac dilation - eccentric growth



## *in silico* prediction of cardiac dilation

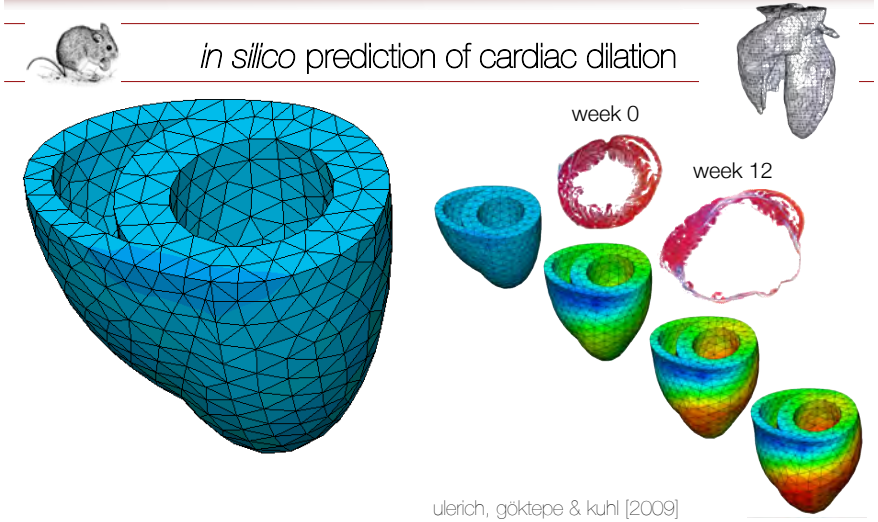


ulerich, göktepe & kuhl [2009]

doyle, sheikh, sheikh, cao, yang, robbins, wu [2007]

## cardiac dilation - eccentric growth

## *in vivo* model of sarcomerogenesis

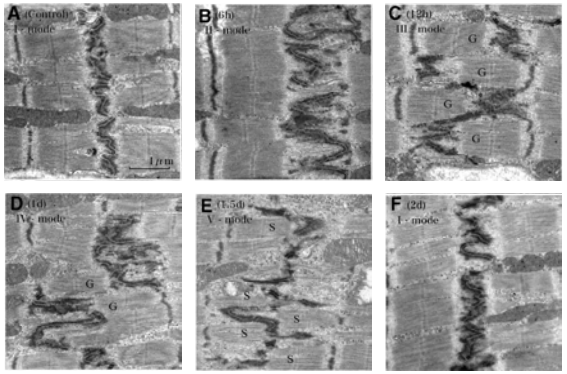


**Figure 10.** Ultrastructural changes of the intercalacted disk after volume overload. A Control. After 6 hours of volume overload, the ICD becomes thick with one-sarcomere-long interdigitations. B After 12 hours, the ICD is folded to form one-sarcomere-deep grooves and contra-grooves with short interdigitations. C At 1 day, interdigitations elongate up to one-sarcomere long in the folded ICD, D, so that the ICD broadens to ~two sarcomere wide. Grooves and contra-groves appear in this mode. At 1.5 days, the ICD is thin with mostly short interdigitations, but one-sarcomere-long interdigitations sporadically appear as spikes. E.There appear spaces surrounded by several spikes. At 2 days, the ICD is thin and flat with short interdigitaitons similar to those of controls, finishing one cycle of serial sarcomere addition.

yoshida, sho, nonjo, takahashi, kobayashi, kawamura, honma, komatsu, sugita, yamauchi, hosoi, ito, masuda [2010]

## cardiac dilation - eccentric growth



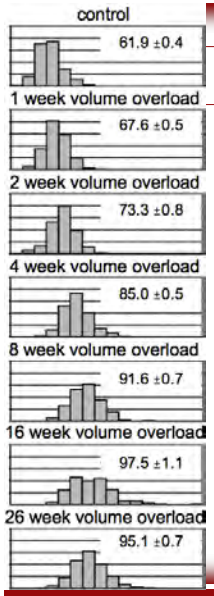


## *in vivo* model of sarcomerogenesis

- **14% dilation** due to volume overload
- dilation by **cardiomyocyte elongation**
- elongation by **serial sarcomere deposition**
- sarcomere **number increases linearly** from 62 to 85
- sarcomere deposition **rate is linear** in weeks 1 to 4 decays smoothly to **saturation** at week 26

yoshida, sho, nonjo, takahashi, kobayashi, kawamura, honma, komatsu, sugita, yamauchi, hosoi, ito, masuda [2010]

## cardiac dilation - eccentric growth



## strain-driven eccentric growth through sarcomerogenesis

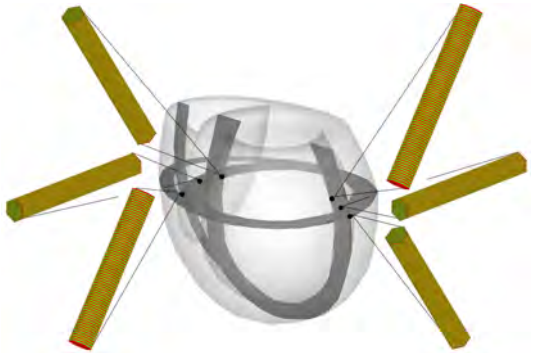

**Figure 7.** Strain-driven eccentric growth. Overall, eccentric growth is clearly hetergeneous with a transmural variation in serial sarcomere deposition. Cardiomyocytes in the endocardium, the inner wall, reach their maximum length of 150μm through the serial deposition of 25 additional sarcomere units of 2μm each. Cardiomyocytes in the epicardium, the outer wall, reach a stable state at a length of 130μm through the serial deposition of 15 additional sarcomere units. Eccentric growth along the septum is almost identical to eccentric growth along the free wall initiating an overall shape change from elliptical to spherical.

goktepe, abilez, parker, kuhl [2010]

## cardiac dilation - eccentric growth



## case III - cardiac wall thickening

- chronic **wall thickening** at constant cardiac size
- wall thickness **increases from 1cm to 3cm**
- cardiomyocyte number remains constant ~6 billion
- cardiomyocyte diameter **increases from 15um to 40um**
- sarcomere number **increases in parallel**
- sarcomere length remains constant at 1.9-2.1um

opie [2003] maron, mc kenna [2003], kumar, abbas, fausto [2005]

## cardiac wall thickening - concentric growth

## case III - cardiac wall thickening

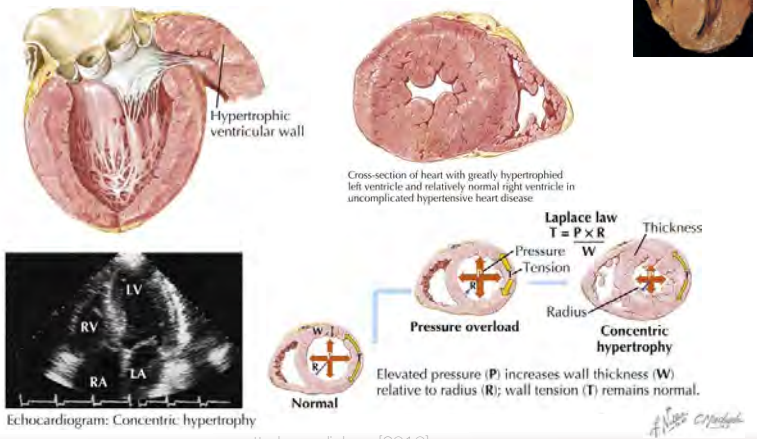


netter's cardiology [2010]

## cardiac wall thickening - concentric growth 37

## constitutive equations

- multiplicative decomposition
  $\boldsymbol{F} = \boldsymbol{F}^{\mathrm{e}} \cdot \boldsymbol{F}^{\mathrm{g}}$ with $\boldsymbol{F} = \nabla_{\boldsymbol{X}} \boldsymbol{\varphi}$
- growth tensor
  $\boldsymbol{F}^{\mathrm{g}} = \boldsymbol{I} + [\,\vartheta^{\mathrm{g}} - 1\,]\, \boldsymbol{s}_0 \otimes \boldsymbol{s}_0$
- evolution of concentric growth multiplier parallel sarcomere deposition rate
  $\dot{\vartheta}^{\mathrm{g}} = k^{\mathrm{g}}(\vartheta^{\mathrm{g}})\, \phi^{\mathrm{g}}(\boldsymbol{M}^{\mathrm{e}})$ with $k^{\mathrm{g}}(\vartheta^{\mathrm{g}}) = \frac{1}{\tau} \left[ \frac{\vartheta^{\max} - \vartheta^{\mathrm{g}}}{\vartheta^{\max} - 1} \right]^{\gamma}$
- growth criterion
  $\phi^{\mathrm{g}} = \mathrm{tr}(\boldsymbol{M}^{\mathrm{e}}) - M^{\mathrm{e\,crit}}$

maximum parallel sarcomere deposition $\vartheta^{\max}$, sarcomere deposition time $\tau$, deposition nonlinearity $\gamma$, critical pressure level $M^{\mathrm{e\,crit}}$

## cardiac wall thickening - concentric growth 38

## algorithmic treatment

| | |
|---|---|
| given $\boldsymbol{F}$ and $\vartheta^{\mathrm{g}}_{\mathrm{n}}$ | |
| initialize $\vartheta^{\mathrm{g}} \leftarrow \vartheta^{\mathrm{g}}_{\mathrm{n}}$ | |
| local Newton iteration | |
| calculate growth tensor $\boldsymbol{F}^{\mathrm{g}} = \boldsymbol{I} + [\,\vartheta^{\mathrm{g}} - 1\,]\, \boldsymbol{s}_0 \otimes \boldsymbol{s}_0$ | (51) |
| calculate elastic tensor $\boldsymbol{F}^{\mathrm{e}} = \boldsymbol{F} \cdot \boldsymbol{F}^{\mathrm{g}\,-1}$ | (1) |
| calculate elastic right Cauchy Green tensor $\boldsymbol{C}^{\mathrm{e}} = \boldsymbol{F}^{\mathrm{e\,t}} \cdot \boldsymbol{F}^{\mathrm{e}}$ | (2) |
| calculate second Piola Kirchhoff stress $\boldsymbol{S}^{\mathrm{e}} = 2\,\partial\psi / \partial \boldsymbol{C}^{\mathrm{e}}$ | (10) |
| check growth criterion $\phi^{\mathrm{g}} = \mathrm{tr}(\boldsymbol{C}^{\mathrm{e}} \cdot \boldsymbol{S}^{\mathrm{e}}) - M^{\mathrm{e\,crit}} \geq 0$ ? | (56) |
| calculate growth function $k^{\mathrm{g}} = [[\vartheta^{\max} - \vartheta^{\mathrm{g}}]/[\vartheta^{\max} - 1]]^{\gamma} / \tau$ | (55) |
| calculate residual $\mathsf{R} = \vartheta^{\mathrm{g}} - \vartheta^{\mathrm{g}}_{\mathrm{n}} - k^{\mathrm{g}}\, \phi^{\mathrm{g}} \Delta t$ | (58) |
| calculate tangent $\mathsf{K} = \partial \mathsf{R} / \partial \vartheta^{\mathrm{g}}$ | (59) |
| update growth multiplier $\vartheta^{\mathrm{g}} \leftarrow \vartheta^{\mathrm{g}} - \mathsf{R} / \mathsf{K}$ | |
| check convergence $\mathsf{R} \leq$ tol ? | |
| calculate second Piola Kirchhoff stress $\boldsymbol{S} = \boldsymbol{F}^{\mathrm{g}\,-1} \cdot \boldsymbol{S}^{\mathrm{e}} \cdot \boldsymbol{F}^{\mathrm{g}}$ | (17) |
| calculate Lagrangian moduli $\mathbf{L}$ | (18) with (19), (20), (53), (60) |
| push forward to Kirchhoff stress $\boldsymbol{\tau} = \boldsymbol{F} \cdot \boldsymbol{S} \cdot \boldsymbol{F}^{\mathrm{t}}$ | (21) |
| push forward to Eulerian moduli $\mathbf{e} = [\,\boldsymbol{F} \otimes \boldsymbol{F}\,] : \mathbf{L} : [\,\boldsymbol{F}^{\mathrm{t}} \otimes \boldsymbol{F}^{\mathrm{t}}\,]$ | (22) |

**Table 3**. Algorithmic treatment of stress-driven transversely isotropic growth.

goktepe, abilez, kuhl [2010]

## cardiac wall thickening - concentric growth 39

## pathophysiology of cardiac wall thickening

**Figure 10**. Stress-driven concentric growth , cardiac wall thickening, and transmural muscle thickening at constant cardiac size, reprinted with permission from Robbins & Cotran. Left ventricular outflow obstruction has caused pressure-overload hypertrophy associated with a significant wall thickening (left). A pronounced septal hypertrophy has caused the significantly thickened septal muscle to bulge into the left ventricular outflow tract (right).

goktepe, abilez, kuhl [2010]

## cardiac wall thickening - concentric growth 40

## cardiac wall thickening through stress-driven concentric growth

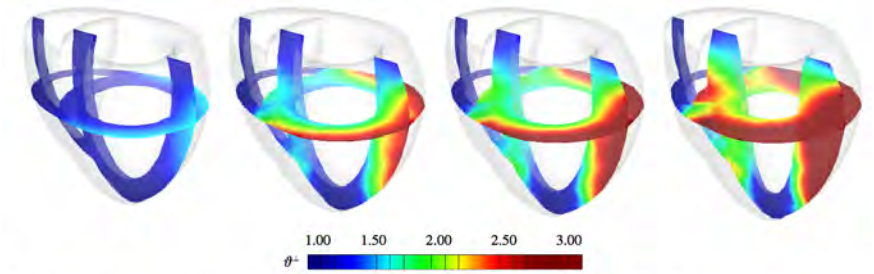


**Figure 10**. Stress-driven concentric growth. The concentric growth multiplier gradually increases from 1.00 to 3.00 as the individual cardiomyocytes grow concentrically. On the structural level, concentric growth manifests itself in a progressive transmural wall thickening to withstand higher blood pressure levels while the overall size of the heart remains virtually unaffected. Since the septal wall receives structural support through the pressure in the right ventricle, wall thickening is slightly more pronounced in the free wall where the wall stresses are higher.

goktepe, abilez, parker, kuhl [2010]

## cardiac wall thickening - concentric growth 41

## cardiac wall thickening through stress-driven concentric growth

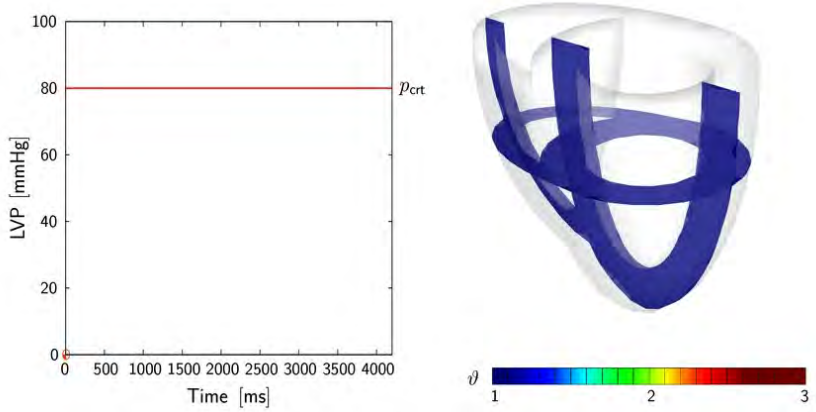


goktepe, abilez, parker, kuhl [2010]

## cardiac wall thickening - concentric growth 42

## stress-driven concentric growth through sarcomerogenesis

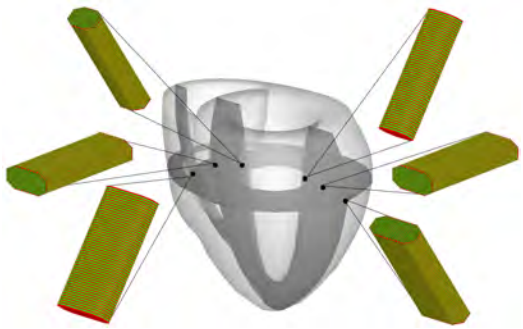

**Figure 9**. Stress-driven concentric growth. Concentric growth is clearly heterogeneous with a transmural variation in parallel sarcomere deposition. Cardiomyocytes in the endocardium, the inner wall, reach a stable state at a thickness of 31.4µm through the parallel deposition of 84 additional sarcomere units. Cardiomyocytes in the epicardium, the outer wall, reach their maximum thickness of 50µm through the parallel deposition of 182 sarcomere units. Concentric growth at the free wall is slightly more pronounced than at the septum.

goktepe, abilez, parker, kuhl [2010]

## cardiac wall thickening - concentric growth 43

## systemic vs pulmonary hypertension

**Figure**. Stress-driven concentric growth, cardiac wall thickening, and transmural muscle thickening at constant cardiac size. Left ventricular wall thickening in response to systemic hypertension (left) from Kumar, Abbas, Fausto [2005]. Right ventricular wall thickening in response to pulmonary hypertension (right), from Padera.

rausch, dam, goktepe, abilez, kuhl [2010]

## cardiac wall thickening - concentric growth 44

## systemic vs pulmonary hypertension

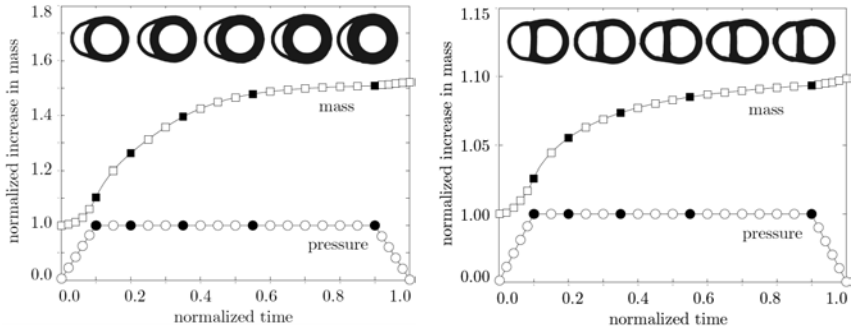


cardiac mass increases more
in systemic (+50%) than in pulmonary (+10%) hypertension

rausch, dam, goktepe, abilez, kuhl [2010]

## cardiac wall thickening - concentric growth 45

## systemic vs pulmonary hypertension

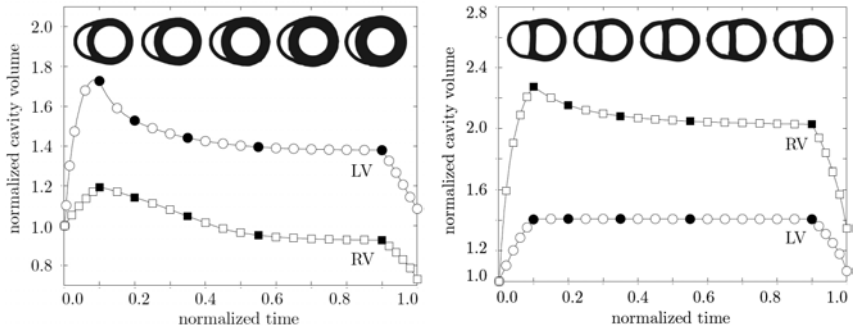


cavity volumes decrease significantly
in both systemic and pulmonary hypertension

rausch, dam, goktepe, abilez, kuhl [2010]

## cardiac wall thickening - concentric growth 46

## systemic hypertension - LV wall thickening

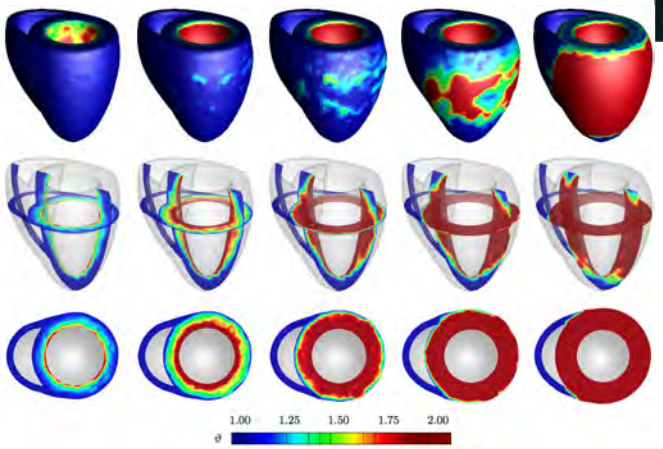


rausch, dam, goktepe, abilez, kuhl [2010]

## cardiac wall thickening - concentric growth 47

## pulmonary hypertension - RV wall thickening

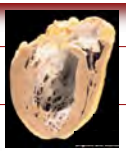

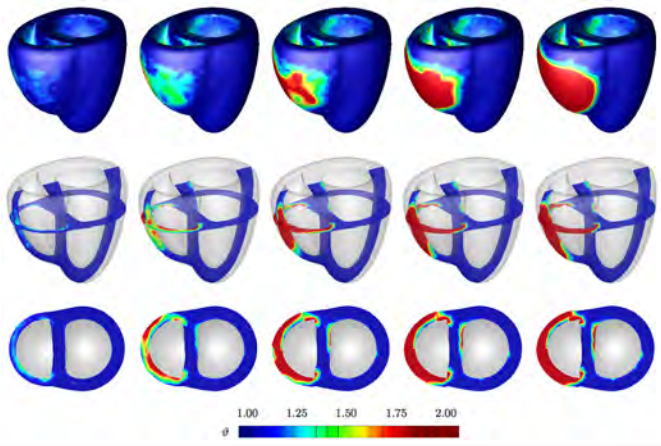


rausch, dam, goktepe, abilez, kuhl [2010]

## cardiac wall thickening - concentric growth 48